Available online at www.sciencedirect.com
ScienceDirect
Journal of Power Sources 165 (2007) 436–445
JOURNAL OF POWER SOURCES
www.elsevier.com/locate/jpowsour

A full model for simulation of electrochemical cells including complex behavior

J.J. Esperilla, J. Félez *, G. Romero, A. Carretero

ETS Ingenieros Industriales, Universidad Politecnica de Madrid, Jose Gutierrez Abascal, 2, 28006 Madrid, Spain

Received 23 July 2005; received in revised form 9 October 2006; accepted 18 November 2006
Available online 16 January 2007

Abstract

This communication presents a model of electrochemical cells developed in order to simulate their electrical, chemical and thermal behavior showing the differences when thermal effects are or not considered in the charge–discharge process. The work presented here has been applied to the particular case of the $Pb,PbSO_4|H_2SO_4$ (aq)$|PbO_2,Pb$ cell, which forms the basis of the lead-acid batteries so widely used in the automotive industry and as traction batteries in electric or hybrid vehicles.

Each half-cell is considered independently in the model. For each half-cell, in addition to the main electrode reaction, a secondary reaction is considered: the hydrogen evolution reaction in the negative electrode and the oxygen evolution reaction in the positive.

The equilibrium potential is calculated with the Nernst equation, in which the activity coefficients are fitted to an exponential function using experimental data. On the other hand, the two main mechanisms that produce the overpotential are considered, that is the activation or charge transfer and the diffusion mechanisms.

First, an isothermal model has been studied in order to show the behavior of the main phenomena. A more complex model has also been studied including thermal behavior. This model is very useful in the case of traction batteries in electric and hybrid vehicles where high current intensities appear.

Some simulation results are also presented in order to show the accuracy of the proposed models.

Keywords: Lead-acid batteries; Electrochemical cells; Thermal behavior; Modeling; Simulation

1. Introduction

The modeling of electrochemical cells, secondary batteries or electrochemical energy storage devices in general has been widely studied, there being a considerable number of previously published works available [1–20]. The large number of works carried out around this topic is partly motivated by the interest aroused by electric and hybrid vehicles. For this reason, many of these works have been developed as a part of simulation models for these vehicles [1–6].

These works are sometimes based on empirical relationships, and other times on a detailed description of the physical and chemical processes that take place in the cell, and even on the development of equivalent circuits [6–8]. In order to develop these models various techniques have been used, such as lookup tables, lumped parameters or bond graphs.

Taking the first works published as a starting point, different extensions and modifications of increasing complexity and precision have gradually been proposed. In some cases [4,9–11] modifications have been made to previously published works [3,12], while in other cases, it has been the authors themselves [13] who have made suggestions for improving their own models [10].

There is also a wide variety depending on the goals. There are isothermal models, for instance, to describe electrochemical cell behavior under normal charge or discharge conditions, models that seek to get as close as possible to the limit current conditions [13], thermal models that include the effect of temperature [1,7,8,14,15], and even age on cell performance [1], models that study the recombination of gases during the charge process, particularly in lead-acid batteries (VRLA) [10,13,16,17],

* Corresponding author. Tel.: +34 91 336 31 16; fax: +34 91 561 86 18.
E-mail addresses: jjesperilla@teleline.es (J.J. Esperilla), jesus.felez@upm.es (J. Félez), gromero@etsii.upm.es (G. Romero), acarretero@etsii.upm.es (A. Carretero).

0378-7753/$ – see front matter © 2006 Elsevier B.V. All rights reserved.
doi:10.1016/j.jpowsour.2006.11.071

or models specially developed to describe cell behavior during a pulse charge/discharge operation [17,18].

A highly interesting alternative for developing these types of models is to use the bond graph technique. This technique allows for the development of models that may belong to different physical domains. This is especially useful to integrate the models developed into other more complex and multidisciplinary ones as, for example, a complete hybrid vehicle model, with all the components like engine, clutch, gear box, chassis, and power system, including the battery and the control system.

In this paper, based on two previous ones by the authors [21,26], a model for an electrochemical cell has been developed. The model has been applied to the particular case of the $Pb,PbSO_4|H_2SO_4$ (aq)$|PbO_2,Pb$ cell. This kind of cell forms the basis of lead-acid batteries that are widely used in the automotive industry as well as traction batteries in electric or hybrid vehicles.

The main goal of this work has been to obtain a model capable of reproducing cell behavior for both charge and discharge conditions. Therefore, an initial isothermal model has been constructed. In many cases, this isothermal model may be sufficient to provide an adequate representation of cell behavior. However, in those cases where high charge currents are involved, the thermal effects may be considerable. A thermal model has also been developed for this case, aimed at providing an adequate representation of these effects.

2. Electrochemistry of the $Pb,PbSO_4|H_2SO_4$ (aq)$|PbO_2,Pb$ cell and bond graph models

2.1. Equilibrium potential and open circuit voltage

Let us consider a cell such as shown in Fig. 1. It consists of a lead electrode (Pb) and another of lead dioxide (PbO_2) submerged in an H_2SO_4 solution. When the two electrodes come together (Fig. 1a), an electric current flows from one to the other due to a potential difference between the two electrodes. The reaction giving rise to this electromotive force is:

$$PbO_2 + Pb + 2H_2SO_4 \rightarrow 2PbSO_4 + 2H_2O \quad (1)$$

This reaction can be split into two parts. One that takes place in the left electrode:

$$Pb + SO_4^{2-} \rightarrow PbSO_4 + 2e^- \quad (2)$$

and the other that takes place in the right one:

$$PbO_2 + 4H^+ + SO_4^{2-} + 2e^- \rightarrow PbSO_4 + 2H_2O \quad (3)$$

The electrode where oxidation occurs is called the anode and the one where reduction occurs is called the cathode. The electromotive force of a galvanic cell is defined as:

$$E = E_c - E_a \quad (4)$$

where E_c and E_a are the reduction potentials of the cathode and the anode, respectively.

If a voltage greater than its electromotive force is applied to the cell, the electrochemical process is inverted in the electrodes (Fig. 1b) and the direction of the reactions (2) and (3) is also inverted.

The dependency of the electromotive force on the concentration of substances taking part in the reaction is given by the Nernst equation:

$$E = E^\circ - \frac{RT}{nF} \ln \prod_i (m_i \gamma_i)^{\nu_i} \quad (5)$$

where E° is the normal or standard electromotive force, R the molar gas constant, T the electrolyte temperature, F Faraday's constant, n the number of electrons exchanged, ν the stoichiometric coefficient, m the molality, and γ is the activity coefficient. In our case, because of the high concentrations of electrolyte used, the solvent activity cannot be considered constant and equal to the unit and must be included. The values of water activity can be obtained, for any concentration of H_2SO_4, from experimental data [22] by adjusting to a polynomial function.

In the case of the electrolytes, owing to the electrically neutral condition, the concentration of one of the ions cannot be varied without changing that of the other, since it is impossible to separate the effects of the positive ions from the negative ones. This means that the activity coefficients of the individual ions cannot be measured experimentally. For this reason the mean

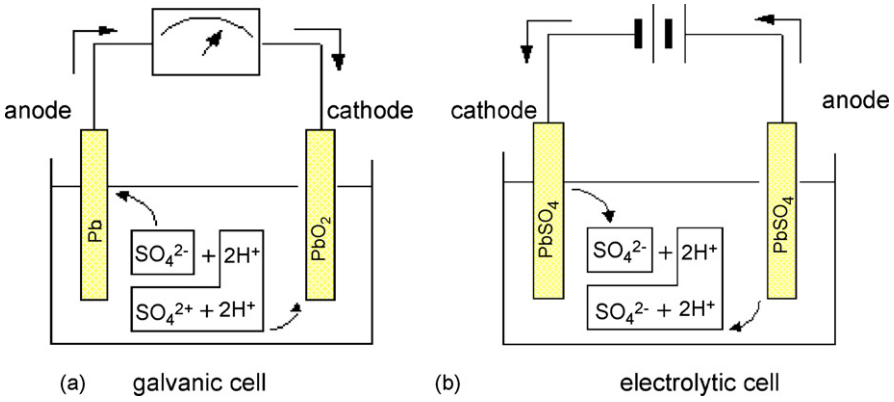

Fig. 1. $Pb,PbSO_4|H_2SO_4$ (aq)$|PbO_2,Pb$ cell.

ionic activity coefficient $\gamma_{\pm}$ is defined as:

$$\gamma_{\pm}^{\nu} = \gamma_{+}^{\nu+} \times \gamma_{-}^{\nu-}; \quad \nu = \nu^{+} + \nu^{-} \tag{6}$$

this being the only coefficient that can be measured experimentally and able to be found in tables. In our case, as the reactions of each electrode are to be looked at individually, it is necessary to have some procedure to estimate the value of the activity coefficients of the positive and negative ions separately. Taking Debye–Hückel's theory for strong electrolytes as a starting point, a relation between these coefficients and the mean ionic activity coefficient can be established:

$$\ln \gamma_{+} = \frac{(\nu/\nu_{-}) \ln \gamma_{\pm}}{(z_{-}/z_{+})^2 + (\nu_{+}/\nu_{-})}; \quad \ln \gamma_{-} \frac{(\nu/\nu_{+}) \ln \gamma_{\pm}}{(z_{+}/z_{-})^2 + (\nu_{-}/\nu_{+})} \tag{7}$$

where z_{+}, y and z_{-} are the charges of the positive and negative ions (in our case SO_4^{2-} and H^{+} ions) and:

$$\gamma_{+} = (\gamma_{\pm})^{1/2}; \quad \gamma_{-} = \gamma_{\pm}^{2} \tag{8}$$

The values of $\gamma_{\pm}$ can be obtained for any concentration of H_2SO_4, from experimental data [22] by adjusting to a polynomial function.

The value given by the Nernst equation corresponds to the reversible electromotive force, that is, when no current is passing through the electrodes or when the current can be considered as negligible and is called open circuit voltage Under the same conditions, the potential of each individual reaction in expression (4) is known as equilibrium potential.

2.2. Overpotential

Under irreversible conditions, that is, when current is flowing through the electrodes, the value for potential is different from that of equilibrium, the difference being known as overpotential, and represented by η. In our case, of all the different mechanisms that can give rise to overpotential, the most important ones are those of charge transfer and diffusion, and only these will be taken into account.

2.2.1. Charge transfer overpotential

Charge transfer overpotential is caused by the charge transfer process between the electrode and the electrolyte through the double layer. The electrochemical kinetics shows its relation to current density by means of Butler–Volmer's equation:

$$\frac{i}{i_0} = \exp\left(\frac{z\alpha F}{RT}\eta_t\right) - \exp\left(-\frac{z(1-\alpha)F}{RT}\eta_t\right) \tag{9}$$

where i_0 is the exchange current density, z the number of electrons exchanged, α the charge transfer coefficient and η_t is the charge transfer overpotential. This relation is shown in Fig. 2 by the solid line, while the dotted lines correspond to each of the addends of expression (9).

However, due to the features of the model, current density has to be used as an independent variable, and, therefore, the inverse relation $\eta_t = f^{-1}(i)$ is necessary which, given the form of (9), cannot be directly calculated. Nevertheless, as can be seen in Fig. 2, for high values of $|\eta_t|$, one of the two addends in (9) can be neglected, thus obtaining Tafel's equations:

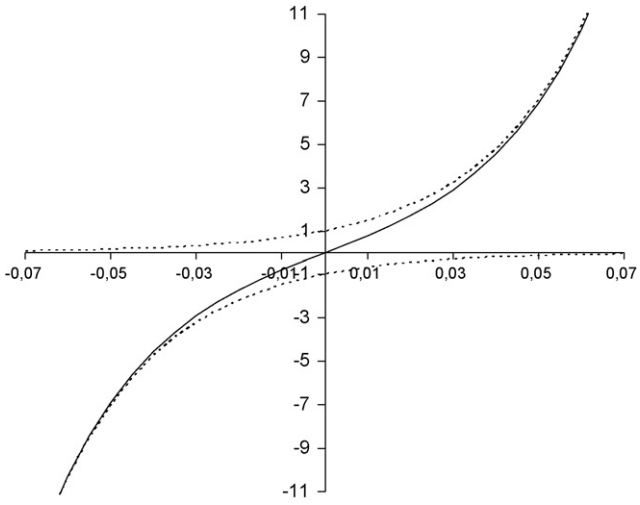

Fig. 2. Current density according to the charge transfer overpotential.

- $\eta_t \gg \frac{RT}{zF}$; $\eta_t > 0$

$$\eta_t = \frac{RT}{z\alpha F} \ln \frac{i}{i_0} \tag{10}$$

- $|\eta_t| \gg \frac{RT}{zF}$; $\eta_t < 0$

$$\eta_t = \frac{RT}{z(1-\alpha)F} \ln \frac{i_0}{|i|} \tag{11}$$

For values of /i/ near to i_0 and lower, the representation of η_t by Tafel's equations is inadequate and leads to a considerable error in η_t. We have chosen to seek a function $i = f(\eta_t)$, with behavior similar to that of (9) in the small value zone of /i/ and that, at the same time, allows to obtain the inverse relation $\eta_t = f^{-1}(i)$.

2.2.2. Diffusion overpotential

When current is flowing through an electrode, the so-called *diffusion layer* is created as a result of the transport of the different species taking part in the reaction from or to the electrode. This layer is a zone where the concentration gradient is other than zero. As a result of this change in concentrations, a difference of potential is caused regarding the equilibrium potential. The corresponding overpotential produced is known as diffusion overpotential.

The diffusion layer takes on a complex profile and is usually substituted by a simpler model, called the *Nernst layer*, where the concentration gradient is taken as constant. By using this approximation, the electrochemical kinetics gives the expression (12) for diffusion overpotential, according to current density, and the density of current limit of each of the species $i_{l,j}$ diffused through the electrode/electrolyte interface:

$$\eta_d = \frac{RT}{nF} \ln \prod_j \left(1 - \frac{i}{i_{l,j}}\right)^{\nu_j} \tag{12}$$

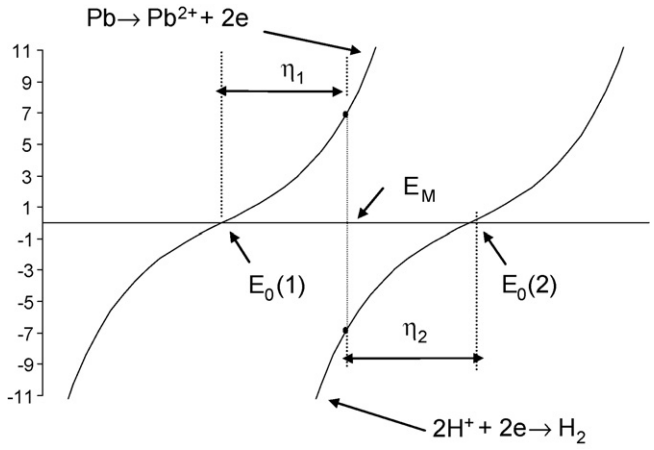

Fig. 3. Mixed potential formation E_M in the anode.

where n in this case, is given by:

$$n = \sum_j \nu_j z_j \tag{13}$$

and where ν_j and z_j are the stoichiometric coefficient and the charge of species j, respectively.

2.3. Secondary reactions and mixed potential

Frequently, two or more processes take place simultaneously in an electrode, as occurs with the anode where, apart from the main reaction, the hydrogen evolution reaction takes place:

$$2H^+ + 2e^- \rightarrow H_2 \tag{14}$$

The current density versus potential behavior curve for the electrode, where the two reactions shown take place, is represented in Fig. 3.

The curve on the left shows the charge transfer process in the electrode main reaction, where η_1 is the overpotential of this reaction, and E_0 (1) is its equilibrium potential. Likewise, η_2 is the overpotential of the reaction (14) and $E_0(2)$ its equilibrium potential. Because the two reactions are independent, the total current density i is obtained by adding the densities of the two reactions, that is:

$$i = i_1 + i_2 \tag{15}$$

in such a way, that when $i = 0$, the potential is neither $E_0(1)$ nor $E_0(2)$, but an intermediate potential E_M, which will be called mixed potential, resulting in:

$$E_0(1) + \eta_1 = E_0(2) + \eta_2 = E_M \tag{16}$$

Likewise, the following secondary reaction occurs in the cathode:

$$H_2O \rightarrow \tfrac{1}{2}O_2 + 2H^+ + 2e^- \tag{17}$$

with oxygen evolution, and with everything commented regarding the anode remaining equally valid.

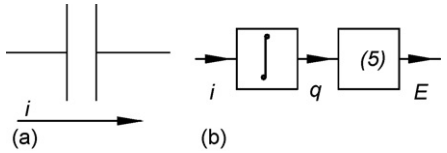

Fig. 4. Equilibrium potential representation.

3. Simulation model

The simulation model has been developed using block diagrams in Simulink, and implementing the equations and dynamic model of the battery in this program. In order to understand the composition of the model, a model with its equivalents in electrical components has been developed that represent the different mechanisms for accumulating potential energy (compliances or capacitors), kinetic (inertances or inductions) or energy dissipation (resistances or resistors). The structure of the model and how the aforementioned electrical equivalents represent the phenomena are described in the above section.

3.1. Isothermal model

The reversible behavior of the cell in respect of the equilibrium potential has been modeled by using a capacitor (Fig. 4a). This element stores free energy, integrating the current intensity (i), in order to obtain the electric charge (q), and thereby obtaining the equilibrium potential by means of Eq. (5), since the electrical charge and molality are directly related by Faraday's laws. Fig. 4b represents the block diagram relative to this element. From Fig. 4 onwards, the number or numbers in brackets placed inside the block refer to the expressions defined in the text of this paper. Thus, starting out from a state of initial charge, and for a positive current, the charge will gradually increase over time, as will the stored electrochemical energy. When the current is negative, the charge will gradually diminish, in the same way as the stored energy. When the state of initial charge is once again reached, the equilibrium potential will also be the same as at the point of departure.

The irreversible behavior of the cell has been represented using a resistance. This element directly relates the current density (i) with the overpotential (η) through expressions (9–12), as is shown in Fig. 5. As a consequence of the principal of the positive production of entropy, the relations between the intensity and overpotential variables must remain in the 1st and 3rd quadrant, as can be seen in Fig. 2. In this way, the potential associated with the resistance will always be positive and represent the dissipated electrical potential.

There should be a capacitor and a resistance for each reaction. Both elements should be joined so that current intensity is

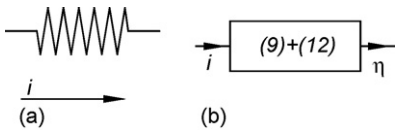

Fig. 5. Overpotential representation.

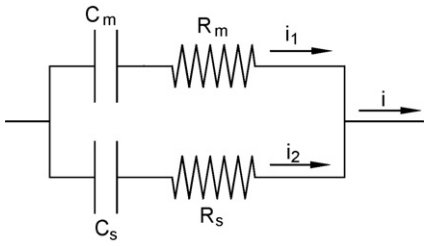

Fig. 6. Main and secondary reactions representation.

the same for both, and the overpotential added to the equilibrium potential. In each electrode, the elements corresponding to each of the reactions (main and secondary) should be joined to one another so that they conform to expressions (15) and (16). Fig. 6 represents the equivalent circuit diagram for the main and secondary reaction.

Finally, the group of elements corresponding to the cathode should be joined to those of the anode so that the current traveling through both will be the same. The electromotive force of the battery will be given by expression (4), where E_c and E_a are the mixed potentials of the cathode and anode, respectively, in line with expression (16). Fig. 7 shows the equivalent electrical diagram and its representation in a block diagram.

3.2. Thermal model

In any chemical reaction, like in those described above, besides the electrochemical energy, there are other energy transformations such as thermal energy and mechanical energy. The Gibb's free energy variation will be expressed by:

$$\mathrm{d}G = -S_{\mathrm{rev}}\,\mathrm{d}T + V\,\mathrm{d}P + E\,\mathrm{d}Q \tag{18}$$

where dT, dp and dQ are temperature, pressure and charge variations, respectively, S_{rev}, V and E the entropy (the part owing to the reversible process), volume and the previously defined equilibrium potential.

A special case would arise when the temperature and pressure remain constant. It can easily be seen from Eq. (18) that under these conditions the changes in the available electrochemical energy arise out of the variations in the Gibb's free energy, the reversible behavior of the cell being able to be represented as set out in Section 3.1.

In general, in a cell like the one described here, it can be taken that any process goes on at constant pressure. In many cases, particularly where there are no very high charge currents, it can be taken that the temperature remains equally constant. However, when the intensity of the current is high, as happens with traction batteries for electric vehicles, the thermal effects can become considerable. Under these circumstances, the temperature cannot be taken as constant. In this case, the reversible behavior of the cell should be represented (maintaining the approximation of constant pressure) using a capacitor where, in addition to a chemical port, like that used in Section 3.1, should be added a thermal port, aimed at taking account of the thermal energy flows produced as a result of the reversible part of the heat reaction, known as the *Peltier effect*.

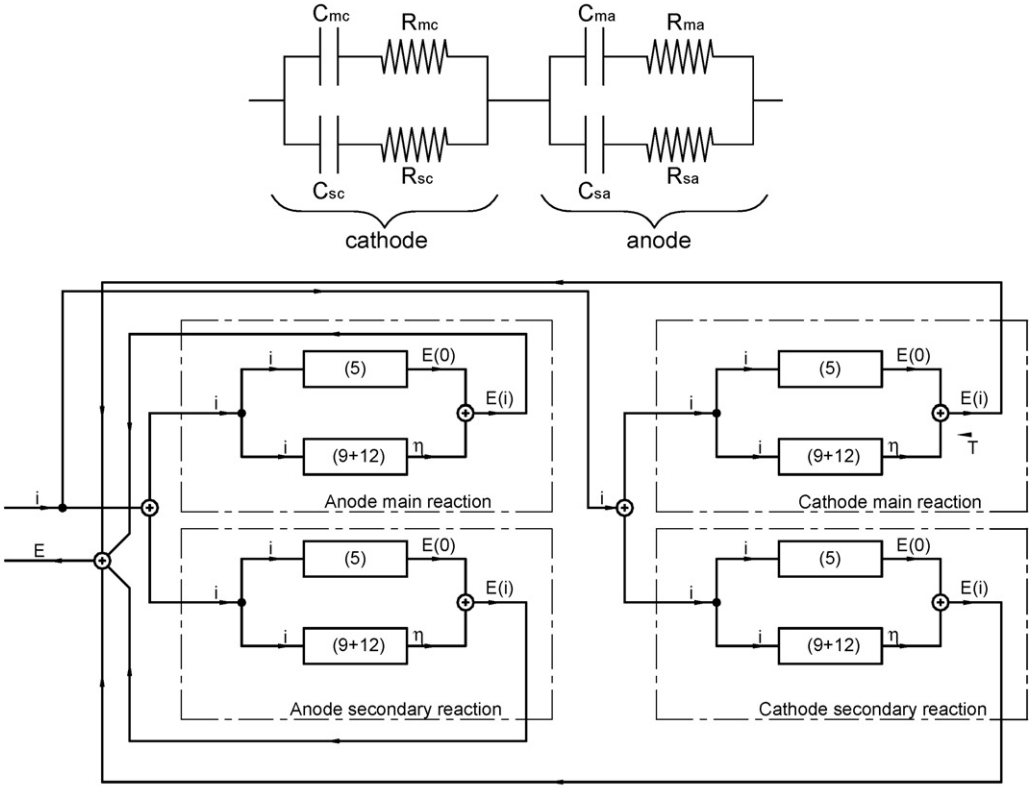

Fig. 7. Full battery representation for the isothermal model.

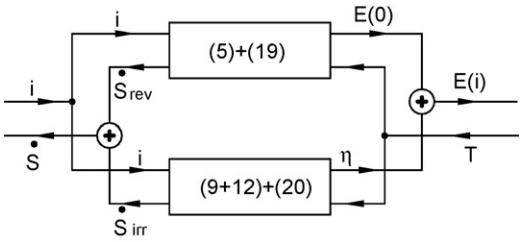

Fig. 8. Block diagram of a chemical reaction considering thermal effects.

Via the thermal port is received the temperature value information, on which, in turn, the equilibrium potential depends, and which serves to calculate the S_{rev} variable using the following constitutive relation:

$$S_{rev} = -\left(\frac{\partial G}{\partial T}\right)_p = Q\left(\frac{\partial E}{\partial T}\right)_p \tag{19}$$

A port must be included in the block diagram, in order to represent the production of entropy as a consequence of the irreversible process (*Joule effect*), in such a way that the thermal potential produced coincides with the electrical potential dissipated:

$$T\dot{S}_{irr} = \eta I \tag{20}$$

where I is the total electrical current due to the electrode reaction. Fig. 8 shows the corresponding block diagram.

The sum of S_{rev} and S_{irr} of each of the electrode reactions will give rise to heating or, circumstantially, due to the reversible process, cooling of the electrolyte. This will act as a thermal accumulator and supply the temperature starting out from the value of the entropy in line with the relation:

$$T = T_{ref}\ \exp\left(\frac{S}{m\,c_v}\right) \tag{21}$$

where T_{ref} stands for the temperature in the initial conditions of the system, m the electrolyte mass and c_v the specific heat per mass at constant volume. For small variations in temperature, and taking the calorific capacity of the electrolyte as constant, it can be established [23] that:

$$T = T_{ref} = T_{ref}\,\frac{S}{m\,c_v} \tag{22}$$

If the temperature T is different from the ambient temperature T_a outside the cell, the electrolyte will exchange heat with the environment surrounding it through the walls of the container in which it is stored. The thermal power exchanged $T\dot{S}_{ext}$ will be given by:

$$T\dot{S}_{ext} = HA(T_a - T) \tag{23}$$

where H is the overall heat transfer coefficient and A is the container's external surface area. If the thermal resistance due to film coefficients of the container's external and internal walls is neglected, H will stand for the heat conduction transfer:

$$H = \frac{k}{\varepsilon} \tag{24}$$

where k is the thermal conductivity of the material and ε the thickness of the container walls.

Fig. 9 shows the complete block diagram of the battery taking account of the above effects.

4. Simulation results

The model developed has been used to represent several situations in order to observe their behavior, particularly with regard to thermal effects, as well as, for contrasting the results with some of those found in literature. Annex I contains the values taken into account in the simulation as well as the references from which they were taken.

Firstly, the charge process of a six element cell coupled in series (corresponding to a standard 12 V. battery) was simulated for two different charge voltages.

Figs. 10–12 show the results of charging a battery at a voltage of 14 V for 2500 s, with an initial electrolyte temperature of 298.15 K. The process was applied to an isothermal model and

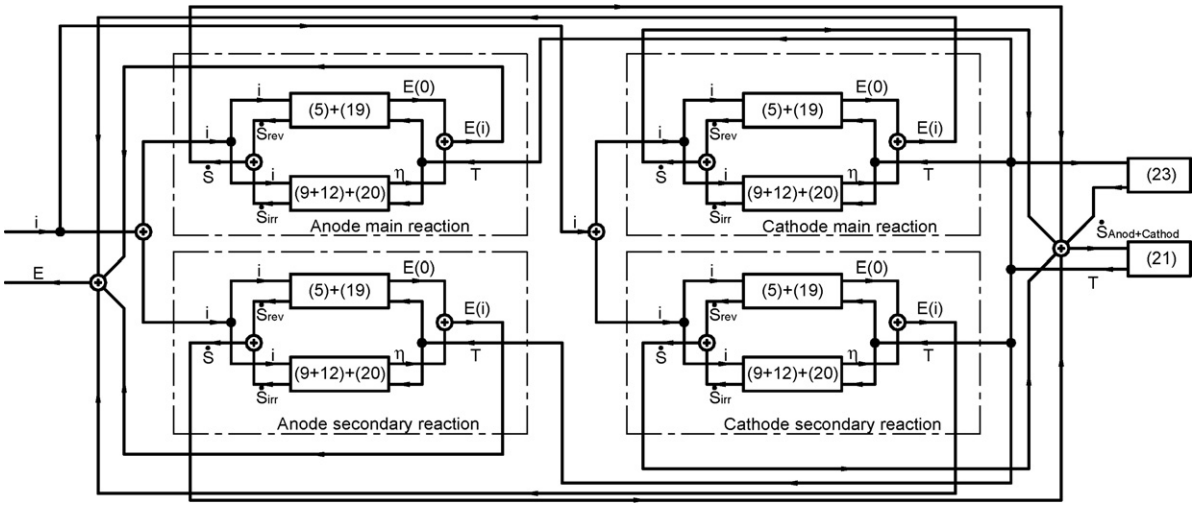

Fig. 9. Complete block diagram of the battery.

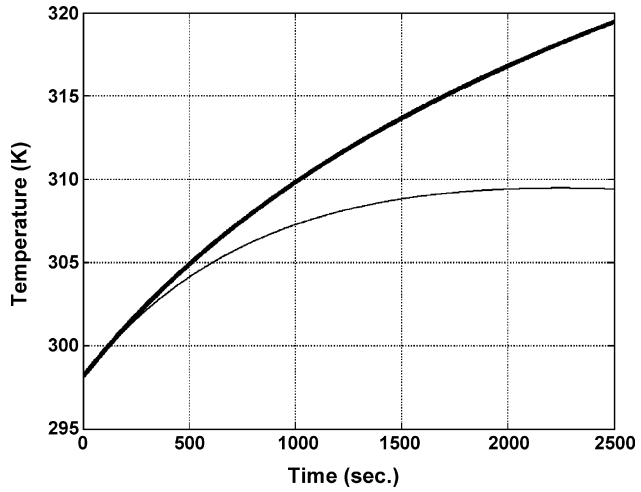

Fig. 10. Temperatures for a 14 V charge. Thick line, adiabatic thermal model. Thin line, non-adiabatic thermal model.

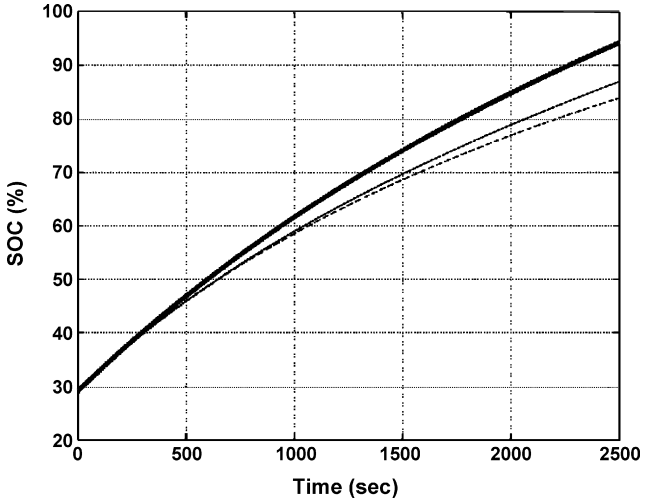

Fig. 11. State of Charge for 14 V charge. Thick solid line, isothermal model. Thin solid line, non-adiabatic thermal model. Dashed line, adiabatic thermal model.

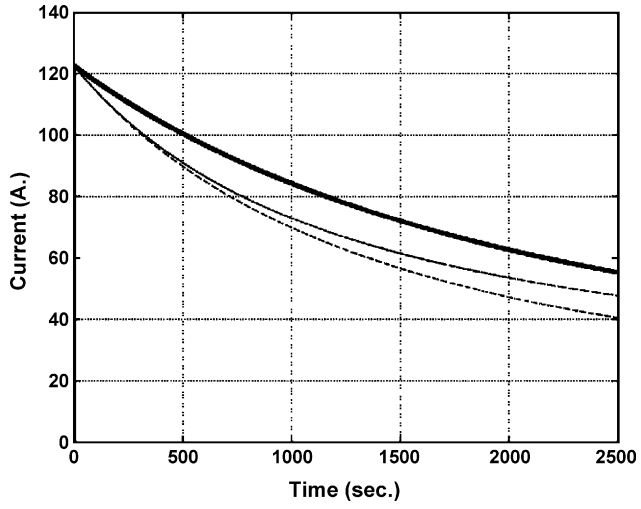

Fig. 12. Charge currents for 14 V charge. Thick solid line, isothermal model. Thin solid line, thermal model. Dashed line, adiabatic thermal model.

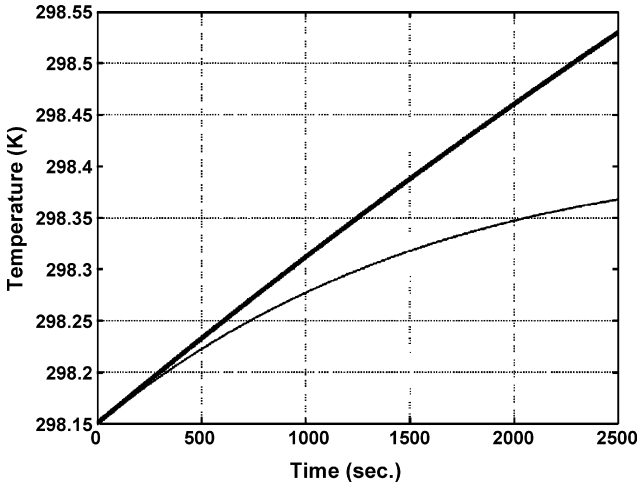

Fig. 13. Temperatures for a 12.2 V charge. Thick solid line, adiabatic thermal model. Thin solid line, non-adiabatic thermal model.

two thermal models. In a thermal model, which we have called the adiabatic model, the battery does not interchange thermal energy with the outside. In the other thermal model, the battery interchanges thermal energy with the outside and we have called it the non-adiabatic model. It can be seen that there are considerable differences depending on the model chosen. In the case where thermal exchange with the outside was taken into consideration, the electrolyte temperature underwent an increase in temperature of 11 K, and 21 K in the other case. The state of charge (SOC) values vary between 94 and 84% at the end of the charge process for both extreme cases. The charge current value at the end of the process is 55 A for the isothermal model, 35.8% greater than for the adiabatic model and 15.1% greater than for the non-adiabatic model.

Likewise, Figs. 13–15 show the results obtained during charging at a voltage of 12.2 V. As can be seen, in this case the charge current is much lower, and as a result the differences among the three models are therefore negligible. The difference found in

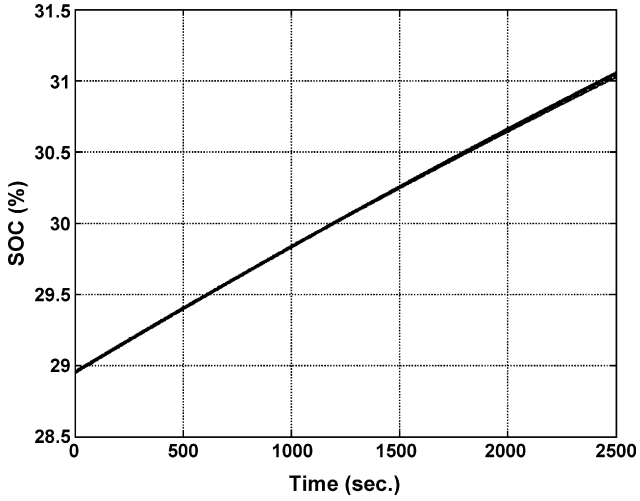

Fig. 14. State of charge for a 12.2 V charge. Thick solid line, isothermal model. Thin solid line, non-adiabatic thermal model. Dashed line, adiabatic thermal model.

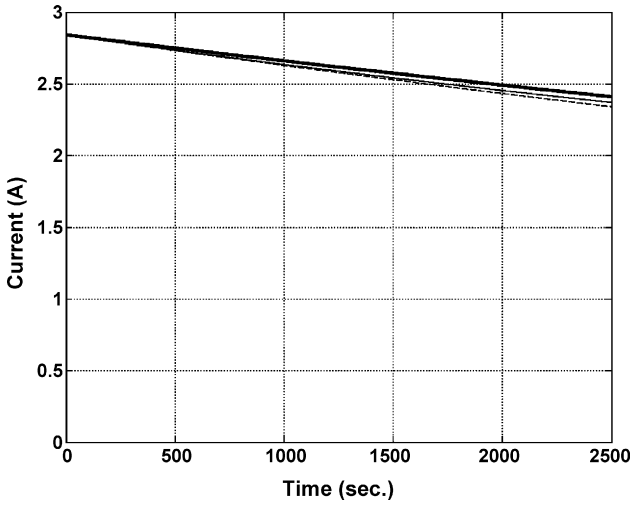

Fig. 15. Charge currents for a 12.2 V charge. Thick solid line, isothermal model. Thin solid line, non-adiabatic thermal model. Dashed line, adiabatic thermal model.

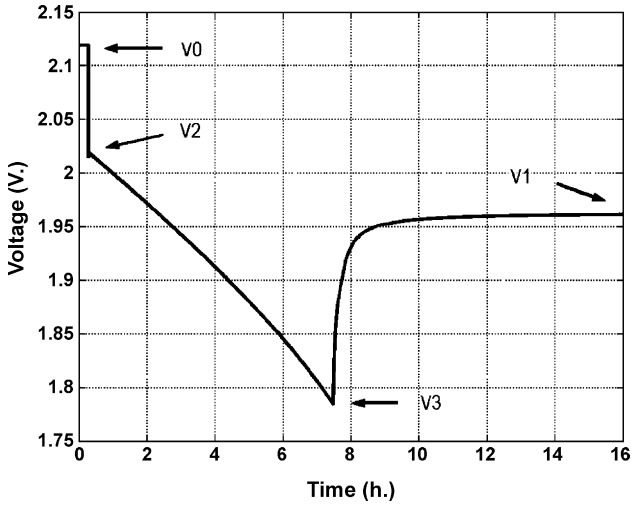

Fig. 16. Discharge voltage for a 63 A current, followed by a period of zero current.

the charge current values at the end of the process was no greater than 3% in the worst case.

5. Model validation

A model of these characteristics is highly dependent on a large number of parameters, not only of an electrochemical nature, but also of a constructive nature (initial electrolyte volume and density, size and internal surface area of the electrode, thermal characteristics of the container material, its surface area in contact with the air, its thickness, . . .). It is, therefore, complicated to validate the model from either experimental or theoretical results found in literature, as the cell or model used as a reference would need to be perfectly defined. It is almost impossible to do this by taking published data. A correct verification of the model would, therefore, require a series of laboratory tests to be carried out. This will be the aim of a future work.

Nevertheless, in order to confirm the good behavior of the model it is necessary that some comparison should be brought to bear with either experimental results or those provided by other sufficiently contrasted models. Ceraolo [7] proposes a model for lead-acid batteries, developed by constructing equivalent electric circuits. This model has been validated with laboratory tests provided by the author himself [8]. This model and the data used for its validation have been used to transfer them to the model developed in this paper and be able to proceed to an initial validation.

The battery used in [7] has a C_{10} capacity of 540 Ah. Once completely charged and stabilized, it was discharged by a 63 A current for a period of 7.197 h, at the end of which time the current remained zero. In order to validate the model developed, the same process was reproduced using the non-adiabatic thermal model presented in this paper. The results relative to the voltage per element supplied by the battery during the discharge process under the conditions described are shown in Fig. 16. As can be seen from Table 1, they coincide fairly closely with those supplied by the experimental results obtained in Ref. [8].

Table 1
Voltage values during the discharge process (see Fig. 10)

	V_0 (V)	V_1 (V)	V_2 (V)	V_3 (V)
Ref. [8]	2.115	1.995	2.01	1.788
This paper	2.119	1.962	2.02	1.786

A discharge at constant current was simulated up to a 1.8 V cut-off voltage per element, in periods of 1, 3 and 10 h (Fig. 17), in order to obtain the values for the capacities for C_1, C_3 and C_{10} and to be able to compare them with those provided by the Ref. [8]. As can be seen in Table 2 and in Fig. 18, the values coincide fairly well.

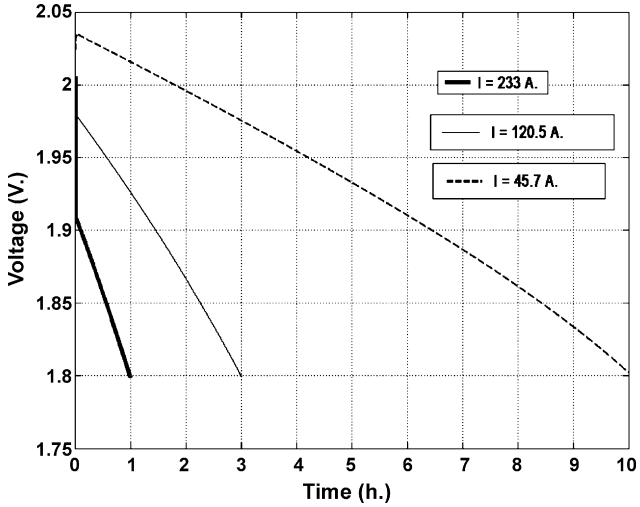

Fig. 17. Discharge voltage at constant current for I_1, I_3 and I_{10}.

Table 2
Data relative to capacity for different discharge rates

	C_1 (Ah)	C_3 (Ah)	C_{10} (Ah)
Ref. [8]	227.5	357	540
This paper	233	361.5	457

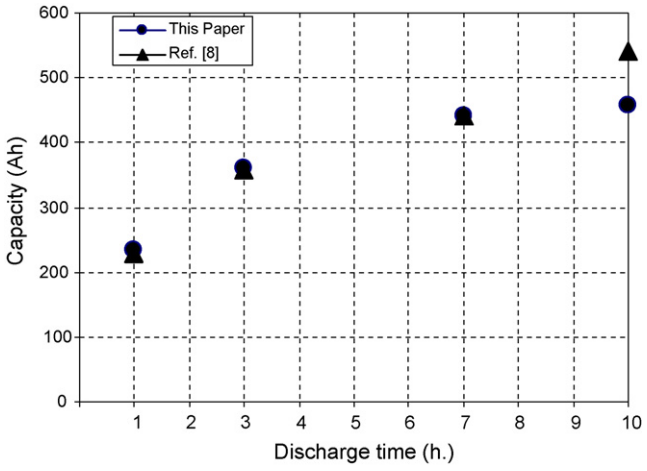

Fig. 18. Capacity vs. discharge time.

6. Conclusions

This work has presented a model of an electrochemical cell including complex behavior, in order to show the different behavior presented in the charging–discharging process of an electrochemical cell.

The charging process for a standard 12 V battery for two different voltage charges was simulated using both the isothermal model and the thermal model. With the latter, it can be seen that when the charge currents are high, the thermal effects are considerable, and at the end of the charge process the electrolyte reaches temperatures considerably higher than at the beginning. This increase in electrolyte temperature has repercussions on the charge current value, and as a result, on the state of charge. Important mistakes can be made if an isothermal model is used. Also, important differences can be seen according to whether the cell's heat exchange with the environment is taken into account or not. It is, therefore, important to make an efficient representation of the heat transmission process between the electrolyte and the environment surrounding the cell.

For those processes where the charge currents are moderate, the thermal effects are not significant, and the differences between both models negligible. This means that in many situations a much simpler isothermal model can be used without committing any significant errors.

Acknowledgements

This work belongs to project TRA99-0919 and DPI2002-2198 and has been developed under the support of the Spanish Administration in the programs of the Ministry of Science and Technology related to Research in Transportation and Design and Industrial Production.

Appendix A. Parameters used during the simulation

Parameter	Value	Ref.
Initial specific surface area for Pb electrode $a_{max,Pb}$ (cm^{-1})	23,000	[20]
Initial specific surface area for PbO_2 electrode a_{max,PbO_2} (cm^{-1})	230,000	[20]
Initial exchange current density $i_{0,max,Pb}$ Eq. (2) ($A\,cm^{-2}$)	4.96×10^{-6}	[20]
Initial exchange current density i_{max,PbO_2} Eq. (3) ($A\,cm^{-2}$)	3.19×10^{-7}	[20]
Initial exchange current density i_{max,H_2} Eq. (14) (A/cm^2)	6.607×10^{-14}	[24]
Initial exchange current density i_{max,O_2} Eq. (17) ($A\,cm^{-2}$)	1.3×10^{-14}	[16]
Initial cell temperature T (K)	298.15	–
Ambient temperature T_a (K)	298.15	–
Standard reduction potential E°_{Pb} Eq. (2) (V)	−0.356	[25]
Standard reduction potential E°_{Pb} Eq. (3) (V)	1.685	[25]
Standard reduction potential $E^{\circ}_{H_2}$ Eq. (14) (V)	0.000	[25]
Standard reduction potential $E^{\circ}_{O_2}$ Eq. (17) (V)	1.229	[25]
Charge transfer coefficient α_{Pb} Eq. (2)	0.775	[20]
Charge transfer coefficient α_{PbO_2} Eq. (3)	0.575	[20]
Charge transfer coefficient α_{H_2} Eq. (14)	0.42	[24]
Charge transfer coefficient α_{O_2} Eq. (17)	0.657	[16]
Exponent for area correction[a], Pb electrode δ_{Pb}	1.5	[5]
Exponent for area correction[a], PbO_2 electrode δ_{PbO_2}	1.5	[5]
Exponent for exchange current density correction[b] ξ_{Pb} Eq. (2)	0.0	[17]
Exponent for exchange current density correction[b] ξ_{PbO_2} Eq. (3)	0.3	[17]
Exponent for exchange current density correction[b] ξ_{H_2} Eq. (14)	1.0	[17]
Exponent for exchange current density correction[b] ξ_{O_2} Eq. (17)	0.0	[17]
Pb electrode size[c,e] V_{Pb} (cm^3)	49	–
Pb electrode size[c,f] V_{PbO_2} (cm^3)	151.9	–
PbO_2 electrode size[c,e] V_{H_2} (cm^3)	49	–
PbO_2 electrode size[c,f] V_{O_2} (cm^3)	151.9	–
Mean ionic activity coefficient $\gamma_{\pm}$	Fitted from ref. data	[22]
Water activity $\chi_{H_2O}\gamma_{H_2O}$	Fitted from ref. data	[22]
Specific heat capacity of electrolyte c_v ($J\,Kg^{-1}\,^{\circ}C^{-1}$)	Fitted from ref. data	[22]

Appendix A (*Continued*)

Parameter	Value	Ref.
Temperature coefficient[d] $\partial E^o_{Pb}/\partial T$ Eq. (2) (from S° tables) ($V\,K^{-1}$)	-1.154×10^{-3}	[25]
Temperature coefficient[d] $\partial E^o_{PbO_2}/\partial T$ Eq. (3) (from S° tables) ($V\,K^{-1}$)	3.27×10^{-4}	[25]
Temperature coefficient[d] $\partial E^o_{O_2}/\partial T$ Eq. (17) (from S° tables) ($V\,K^{-1}$)	-8.46×10^{-4}	[25]
Thermal conductivity of container k ($W\,m^{-1}\,^\circ C^{-1}$)	0.2	–
Thickness of container walls ε (m)	0.005	–
External surface area of container[e] A (m^2)	0.26	–
External surface area of container[f] A (m^2)	1.03	–
Electrolyte volume/element[e] (l)	1.0	–
Electrolyte volume/element[f] (l)	5.25	–
Maximum electrolyte density[e,f] ($Kg\,l^{-1}$)	1.28	–
Maximum electrolyte concentration[b] $[SO_4H_2]_{max}$ ($mol\,Kg^{-1}$)	6.08	–

[a] The specific surface area for each electrode changes with SOC so that: $a_j = a_{max,j}(1 - Q/Q_{max})\delta_j$ for charge, and $a_j = a_{max,j}(Q/Q_{max})\delta_j$ for discharge; j = Pb,PbO_2.

[b] The exchange current density changes for each reaction with the concentration of acid $[SO_4H_2]$, so that: $i_{0,j} = i_{0,max,j}([SO_4H_2]/[SO_4H_2]_{max})^{\xi_j}$; j = Pb, PbO_2, H_2, O_2.

[c] Current intensity I for any reaction is related to the corresponding current density i, the specific surface area, and the size of the electrode V by means of: $I_j = i_j a_j V_j$; j = Pb, PbO_2, H_2, O_2.

[d] To calculate S_{rev} using expression (19), taking as reference value that corresponding to Eq. (14).

[e] Values corresponding to the results in Figs. 10–15.

[f] Values corresponding to the results in Figs. 16–18 and Tables 1 and 2.

References

[1] V.P. Roan, A. Raman, Proceedings of the 28th Intersociety Energy Conversion Engineering Conference, vol. 8, 1993, pp. 2229–2237.

[2] K.E. Bailey, B.K. Powell, Proceedings of the 1995 American Control Conference, vol. 6, 1995, pp. 1677–1682.

[3] P. Ekdunge, J. Power Sources 46 (1993) 251–262.

[4] G.A. Hubbard, K. Youcef-Toumi, Proceedings of the 1997 American Control Conference, vol. 6, 1997, pp. 636–640.

[5] J.N. Harb, V.H. Johnson, D. Rausen, Tutorials Electrochem. Eng.-Math. Model. 14 (1999) 163–177.

[6] B.K. Powell, T.E. Pilutti, Proceedings of the 33rd IEEE Conference on Decision and Control, vol. 12, 1994, pp. 2736–2750.

[7] M. Ceraolo, IEEE Trans. Power Syst. 15 (2000) 1184–1190.

[8] S. Barsali, M. Ceraolo, IEEE Trans. Energy Convers. 17 (2002) 16–23.

[9] D.M. Bernardi, A.Y. Schoene, H. Gu, J. Electrochem. Soc. 140 (1993) 2250–2257.

[10] D.M. Bernardi, M.K. Carpenter, J. Electrochem. Soc. 142 (1995) 2631–2641.

[11] T.V. Nguyen, R.E. White, Electrochim. Ada 38 (1993) 935–945.

[12] W. Tiedemann, J. Newman, Proceedings of the Symposium on Battery Design and Optimization, vol. 1, 1979, pp. 23–38.

[13] D.M. Bernardi, R.Y. Ying, P.L. Watson, 204th Meeting of The Electrochemical Society, vol. 205–210, 2003 (Abstract).

[14] D. Karnopp, J. Franklin Inst. 327 (1990) 983–992.

[15] W.B. Gu, C.Y. Wang, J. Electrochem. Soc. 147 (2000) 2910–2922.

[16] J. Newman, W. Tiedemann, J. Electrochem. Soc. 144 (1997) 3081–3090.

[17] V. Srinivasan, G.Q. Wang, C.Y. Wang, J. Electrochem. Soc. 150 (2003) A316–A325.

[18] R.M. La Follette, D. Benion, J. Electrochem. Soc. 137 (1990) 3701–3707.

[19] J. Thoma, Simul. Pract. Theory 7 (1999) 613–622.

[20] T.V. Nguyen, R.E. White, H. Gu, J. Electrochem. Soc. 137 (1990) 2998–3003.

[21] J.J. Esperilla, C. Vera, J. Félez, J.M. Mera, Proceedings of the ICBGM'2003. Simulation Series, vol. 35, 2003, pp. 293–299.

[22] H. Bode, Lead Acid Batteries, Wiley and Sons, New York, NY, 1977.

[23] J. Thoma, B. Ould Bouamama, Modelling and Simulation in Thermal and Chemical Engineering, Springer-Verlag, Berlin, 1999.

[24] L.T. Lam, J.D. Douglas, R. Pillig, D.A.J. Rand, J. Power Sources 48 (1994) 219–232.

[25] R.C. Weast, M.J. Astle, Handbook of Chemistry and Physics, CRC Press, Inc., Florida, 1981.

[26] J.J. Esperilla, C. Vera, J. Félez, J.M. Mera, Proceedings of the ICBGM'2005. Simulation Series 37 no. 1, 2003, pp. 255–261.